Appendix I:

Xu, F., El-Leathy, A.M., Kim, C.-H. and Faeth, G.M. (2003) "Soot Surface Oxidation in Laminar Hydrocarbon/Air Diffusion Flames at Atmospheric Pressure," *Combust. Flame*, in press.

SOOT SURFACE OXIDATION IN HYDROCARBON/AIR DIFFUSION FLAMES AT ATMOSPHERIC PRESSURE

F. Xu , A.M. El-Leathy, C.H. Kim and G. M. Faeth*
Department of Aerospace Engineering
The University of Michigan
Ann Arbor, MI 48109-2140, U.S.A.

Soot surface oxidation was studied experimentally in laminar hydrocarbon/air diffusion flames at atmospheric pressure. Measurements were carried out along the axes of round fuel jets burning in coflowing dry air considering acetylene-nitrogen, ethylene, propyiene-nitrogen, propane and acetylene-benzene-nitrogen in the fuel stream. Measurements were limited to the initial stages of soot oxidation (carbon consumption less than 70%) where soot oxidation occurs at the surface of primary soot particles. The following properties were measured as a function of distance above the burner exit: soot concentrations by deconvoluted laser extinction, soot temperatures by deconvoluted multiline emission, soot structure by thermophoretic sampling and analysis using Transmission Electron Microscopy (TEM), concentrations of major stable gas species (N_2, H_2O, H_2, O_2, CO, CO_2, CH_4, C_2H_2, C_2H_4, C_2H_6, C_3H_6, C_3H_8, and C_6H_6) by sampling and gas chromatography, concentrations of some radical species (H, OH, O) by deconvoluted Li/LiOH atomic absorption and flow velocities by laser velocimetry. For present test conditions, it was found that soot surface oxidation rates were not affected by fuel type, that direct rates of soot surface oxidation by O_2 estimated from Nagle and Strickland-Constable (1962) were small compared to observed soot surface oxidation rates because soot surface oxidation was completed near the flame sheet where O_2 concentrations were less than 3% by volume, and that soot surface oxidation rates were deseribed by the OH soot surface oxidation mechanism with a collision efficiency of 0.14 and an uncertainty (95% confidence) of ± 0.04 when allowing for direct soot

---

*Corresponding author. E-mail: gmfaeth@umich.edu surface oxidation by O_2, which is in reasonably good agreement with earlier observations of soot surface oxidation rates in both premixed and diffusion flames at atmospheric pressure.

NOMENCLATURE

C_i	mass of carbon oxidized per mole of species i reacted (kg/kgmol)
d	fuel port exit diameter (m)
d_p	mean primary soot particle diameter (m)
f_s	soot volume fraction (-)
Fr	burner exit Froude number (-), $u_o^2/(gd)$
g	acceleration of gravity (ms^{-2})
[i]	molar concentration of species i (kgmole m^{-3})
M_i	molecular weight of species i (kg $kgmol^{-1}$)
n_p	number of primary particles per unit volume (m^{-3})
Re	burner exit Reynolds number (-), $u_o d/\nu_o$
R_u	universal gas constant (J $kgmol^{-1}$ K^{-1})
S	soot surface area per unit volume (m^{-1})
t	time (s)
T	temperature (K)
u	streamwise velocity (m s^{-1})
$\bar{v}_i$	mean molecular velocity of species i (m s^{-1})
w_{ox}	soot surface oxidation rate (kg $m^{-2}s^{-1}$)
z	streamwise distance (m)

Greek Symbols

η_i	collision efficiency of species i
ν	kinematic viscosity ($m^2 s^{-1}$)

ρ	gas density (kg m^{-3})
ρ_s	soot density (kg m^{-3})
ϕ	fuel-equivalence ratio (-)

Subscripts

o	burner exit condition

INTRODUCTION

Soot is an important unsolved combustion problem because it is present in most hydrocarbon-fueled flames and current understanding of the reactive and physical processes of soot in flame environments is limited. In particular, lack of knowledge about soot formation and oxidation in flames affects progress toward developing reliable predictions of flame radiation properties, predictions of flame pollutant emission properties and methods of computational combustion, among others. Motivated by these observations, the present investigation extended past experimental studies of soot formation in laminar premixed and diffusion flames in this laboratory [1-7], to consider soot surface oxidation in laminar diffusion flames using similar methods. The following description of the research is brief, more details and a complete tabulation of the measurements are provided by Xu [8] and El-Leathy [9].

Potential soot surface oxidants in hydrocarbon-fueled diffusion flames include O_2, CO_2, H_2O, O and OH. Numerous simplified treatments have been reported that can be used to estimate soot surface oxidation rates in frequently-encountered instances when local radical concentrations are not known [10-18]. Present emphasis, however, is on the potential contributions of both stable and radical species to soot surface oxidation.

The results of the classical study of the surface oxidation of pyrolytic graphite by O_2, due to Nagle and Strickland-Constable [10], have been shown to be effective for estimating the surface oxidation rates of soot by O_2, as well, based on the measurements of Radcliffe and Appleton [13] and Park and Appleton [14] (other studies of soot surface oxidation by O_2 will be discussed later). Subsequent work by Fenimore and Jones [19] and Mulcahy and Young [20], however, showed that soot surface oxidation in flame environments having relatively small O_2 concentrations substantially exceeded estimates based on the results of Nagle and Strickland-Constable [10], prompting suggestions that radicals such as O and particularly OH might be strong contributors to soot surface oxidation rates for such conditions. Prompted by this suggestion, Neoh and coworkers [21-23] carried out measurements of soot surface oxidation rates in premixed flames considering conditions involving temperatures of 1575-1865 K and O_2 concentrations less than 5% by volume at atmospheric pressure. They found that O_2, CO_2, H_2O and O were not significant contributors to soot surface oxidation at these conditions and that OH was the principle surface oxidant of soot instead. They reported a collision efficiency of 0.27 with an uncertainty (95% confidence) of ± 0.06 when soot particle surface area was found using optical scattering and extinction measurements and a collision efficiency roughly half as large, 0.13 with an uncertainty (95% confidence) of ± 0.03 when accounting for the actual structure of the soot particles as aggregates of spherical and nearly monodisperse primary soot particles based on transmission electron microscopy (TEM) measurements of the structure of soot particles collected on a quartz probe (note that the uncertainties of the mean collision efficiencies just given were found from the measurements reported by Neoh et al. [21] during the present investigation). They suggested that the actual value of the OH collision efficiency was between these limiting values. Later studies by Wicke et al. [24,25] and Roth et al. [26], who considered soot surface oxidation in homogeneous environments, confirmed the findings of Neoh and coworkers [21-23] within experimental uncertainties.

Due to its importance for most practical applications, there have been several investigations of soot surface oxidation within diffusion flames. This has included measurements of soot surface oxidation rates in round methane jet diffusion flames burning in coflowing air due to Garo et al. [27,28]; in round methane, methane-butane and methane-1-butane jet diffusion flames burning in coflowing air due to Puri et al. [29,30]; and in plane methane-nitrogen jet diffusion flames burning in a coflowing argon-oxygen mixture above a Wolfhard-Parker burner due to Haudiquert et al. [31]. These studies did not evaluate CO_2, H_2O and O as potential soot surface oxidizers; nevertheless, they still concluded that OH dominated the mechanism of soot surface oxidation in flames when oxidation was completed near the flame sheet. Garo et al. [27,28] considered a temperature range of 1800-1850 K at atmospheric pressure for conditions where direct rates of soot surface oxidation by O_2, estimated using the results of Nagle and Strickland-Constable [10], were small. Their results were based on optical scattering and extinction measurements to find soot particle surface areas and yielded a mean OH collision efficiency of 0.06 with an uncertainty (95% confidence) of ± 0.04 (again, the uncertainty was computed during the present investigation from the measurements reported by Garo et al. [27,28]). This value is of the same order of magnitude as the results of Neoh and coworkers [21-24] for premixed flame environments but still is significantly smaller than the value of their collision efficiency that was similarly based on optical determinations of soot particle surface areas. Puri et al. [29,30] considered the temperature range 1240-1780 K at atmospheric pressure for their three fuels but unfortunately had to conclude that accurate values of the collision efficiencies for soot surface oxidation due to OH could not be obtained from their data. Finally, Haudiquert et al. [31] considered a temperature range higher than the rest, 2200-2600 K, at atmospheric pressure for conditions where direct rates of soot surface oxidation, estimated using the results of Nagle and Strickland-Constable [10], were small. Their results were based on optical scattering and extinction determinations of soot particle surface areas and yielded OH collision efficiencies of roughly 0.10 and 0.01 at the lower and upper temperature extremities of their test conditions. Thus, the results at the lower end of their temperature range are comparable to the measurements of Garo et al. [27,28] but are significantly smaller than the measurement of Neoh and coworkers [21-23], both based on optically determined soot particle surface areas. An explanation for this discrepancy is that the optical scattering and extinction method for estimating soot particle surface area is based on models that have not been very successful for representing the optical properties of soot [32,33]. As a result, differences of the structure of the various soot populations present at the test conditions of Neoh and coworkers [21-23], Garo et al. [27,28] and Haudiquert et al. [31] may not have been accurately represented by the optical models when soot surface areas were found, affecting OH collision efficiencies accordingly. Direct evidence for difficulties along these lines is provided by the different OH collision efficiencies for soot surface oxidation mentioned earlier found by Neoh and coworkers [21-23] using the optical and sampling/TEM determinations of soot particle surface areas. Supporting evidence is that use of optical methods to find soot particle surface areas during early studies of soot surface growth in fuel-rich premixed flames has proven to be problematical, see Xu et al. [4,5] and references cited therein. Whatever the source of the problem, however, these differences between observations of soot surface oxidation in premixed and diffusion flames clearly should be resolved.

Based on the preceding review of the literature, the present investigation sought to contribute to better understanding of soot surface oxidation properties in laminar diffusion flames with the following specific objectives: (1) to complete measurements of soot properties (soot volume fractions and primary particle diameters) and flame structure properties (temperatures, stable and radical species concentrations, and velocities) within the soot surface oxidation region of several laminar hydrocarbon-fueled diffusion flames, and (2) to exploit the new measurements to evaluate potential soot surface oxidation mechanisms, attempting to resolve the discrepancies between OH collision efficiencies found for premixed and diffusion flames that were just discussed. The experiments were limited to measurements along the axes of laminar coflowing jet diffusion flames burning in air at atmospheric pressure and fueled with various hydrocarbons, similar to the flames used by Xu and El-Leathy and coworkers [7-9] to study soot formation in laminar diffusion flames. The particular hydrocarbon fuels considered included representative alkynes, alkenes, alkanes and aromatics in order to investigate effects of various families of hydrocarbons on soot surface oxidation properties, e.g., acetylene, ethylene, propylene, propane and benzene. Present considerations were limited to the early stages of soot oxidation (carbon consumption less than 70%) where reaction at the surface of primary soot particles dominates the process, rather than the later stages where porosity and internal oxidation of the primary soot particles become important as discussed by Neoh et al. [23].

EXPERIMENTAL METHODS

The test apparatus and instrumentation were unchanged from the earlier study of soot formation in laminar diffusion flames [7] and will be described only briefly. The test flames involved laminar jet diffusion flames having a dry air coflow using a flat honeycomb burner (note, the present dry air consisted of 21% O_2 and 79% N_2 by volume, thus avoiding problems of argon eluting with O_2 during gas chromatography measurements as well as contamination of the flame by the small levels of CO_2 and water vapor that are present in natural air). The honeycomb burner had 1 mm cell sizes that were 20 mm long. The burner consisted of a 35 mm diameter inner port for the fuel-containing stream and a 60 mm diameter coannular outer port for the air coflow, both directed vertically upward. The combustion products were removed using a blower that had an inlet diameter of 125 mm located roughly 800 mm above the burner exit. The flames burned in the dry air coflow with room disturbances controlled by surrounding the flames with several layers of screens and a plastic enclosure. The burner could be traversed in the vertical and horizontal directions to accommodate rigidly-mounted optical instrumentation.

Soot volume fractions were found by deconvoluting laser extinction measurements at 632.8 nm for chord-like paths through the flames, using the refractive indices of Dalzell and Sarofim [34] for consistency with past work in this laboratory [1-7]. Correction of the present results to any future improved refractive indices, however, involves only a simple ratio of the values used here and the new values. Finally, the values used here have recently been confirmed by Krishnan et al. [35]. The experimental uncertainties (95% confidence) of these measurements are estimated to be less than 10% for soot volume fractions greater than 0.02 ppm, increasing inversely proportional to the soot volume fraction for smaller values.

Soot temperatures were found by deconvoluting spectral radiation intensities for chord-like paths through the flames and computing temperatures from measurements at wavelength pairs of 550/700, 550/750, 550/830, 600/700, 600/750, 600/830 and 650/750 nm. Temperature differences between the average and any of the line pairs were less than 50-100 K and experimental uncertainties (95% confidence) of these measurements were less than 50 K.

Concentrations of stable gas species were measured using isokinetic sampling and analysis by gas chromatography, seeking concentrations of N_2, H_2O, H_2, O_2, CO, CO_2, CH_4, C_2H_2, C_2H_4, C_2H_6, C_3H_6, C_3H_8, C_6H_6 and neon (the last being a tracer gas used to estimate effects of radial diffusion of lithium-containing species that were used to find H concentrations). The experimental uncertainties (95% confidence) of these measurements are estimated to be less than 10% for stable gas species having concentrations greater than 0.1 %, increasing to roughly 30% at the present limit of detection of stable gas species, brought to this level by repeated measurements to establish accurate calibrations as well as reliable average concentration values for each species.

Soot primary particle diameters were measured using thermophoretic sampling and analysis by Transmission Electron Microscopy (TEM). Thermophoretic soot sampling results are only reported here for locations along the axes of the flames. The fact that these samples were not contaminated by the sampler passing through off-axis soot-containing regions when moving to-and-from the flame axis was established in two ways, as follows: (1) sampling in the region prior to the onset of soot formation along the axes of the flames (but where there was a well-developed annular soot-containing region near the edge of the region exhibiting yellow soot luminosity) properly indicated that no soot aggregates, that could have been deposited as the sampler passed through the annular soot-containing region, were present on the sampler for the sampling conditions used during the present study, and (2) the sampled soot exhibited nearly constant primary soot particle diameters at each flame condition along the axis (the standard deviations of primary particle diameters at a given point along the axis were less than 10%) rather than the widely-varying primary soot particle diameters that would be observed if off-axis soot particles were present in the sample. The experimental uncertainties (95% confidence) of mean primary soot particle diameters at a point were estimated to be less than 10%.

Streamwise gas velocities were measured using laser velocimetry. The experimental uncertainties (95% confidence) of these measurements were estimated be less than 5%.

Finally, H concentrations were measured using the Li/LiOH atomic absorption method similar to Neoh and coworkers [21-23] which involved deconvoluted atomic absorption measurements with corrections for radial diffusion of lithium-containing species, as discussed earlier. Corresponding measurements of H concentrations in a methane/oxygen premixed flame were used to calibrate the H concentration measurements, similar to Neoh and coworkers [21-23] as discussed by Xu and Faeth [6]. Experimental uncertainties (95% confidence) of the H concentration measurements are estimated to be less than 30%. Given measured concentrations of H, O_2, H_2 and H_2O, values of O and OH concentrations were computed assuming partial equilibrium among these species following Neoh et al. [21,22] using equilibrium constant data from Chase et al. [36]. This involved finding O and OH concentrations assuming partial equilibrium considering H, H_2O and H_2 concentrations for fuel-rich conditions and H, H_2O and O_2 concentrations for fuel-lean conditions. Thus, experimental uncertainties of O and OH were comparable to those of H. The laminar premixed flame used to calibrate the H concentration measurements operated using the fuel port of the present burner, see Xu and Faeth [6] for a summary of the properties of this flame.

The present test flames consisted of three acetylene-nitrogen/air laminar jet diffusion flames, that were identical to those considered during the earlier soot formation study [7], and six new flames involving hydrocarbons other than acetylene, e.g., ethylene/air, propylene-nitrogen/air, propane/air flames and these acetylene-benzene-nitrogen/air flames. When necessary, nitrogen dilution of the fuel stream was used to limit maximum soot concentrations in the flames to values less than 2 ppm, in order to avoid measurement problems due to the presence of large soot concentrations.

The general operating properties of all nine test flames are summarized in Table 1. A dark-field photograph of one of the flames (Flame 4, the ethylene/air flame) appears in Fig. 1; it is similar in appearance to the other flames. Similar to the flame illustrated in Fig. 1, all the flames were steady and attached close to the honeycomb at the burner exit. Except at their base where no soot was present and the flames were blue, the flames were yellow due to luminosity from hot soot particles. The yellow luminous flame length (see Table 1) was approximately equal to the stoichiometric flame length (where the local fuel-equivalence ratio was unity along the flame axis) but was slightly shorter than the stoichiometric flame length for the acetylene-nitrogen/air and acetylene-benzene-nitrogen/air flames (due to early burn out of soot at fuel-rich conditions) and slightly longer than the stoichiometric flame length for flames fueled with the other hydrocarbons (due to delayed burn out of soot at fuel-lean conditions). The present measurements were confined to the portion of the soot surface oxidation region of the test flames that was located at fuel-rich conditions. The stoichiometric flame temperatures in Table 1 were found from adiabatic combustion calculations using the algorithm of McBride et al. [37]. Finally, potential problems of acetone contamination of acetylene, noted by Hamins et al. [38] and Colket et al. [39,40] are not thought to be a problem for present measurements, as discussed by Xu and Faeth [7].

RESULTS AND DISCUSSION

Flame Structure

Typical TEM photographs of soot samples collected from the present flames are illustrated in Fig. 2. These results were obtained along the axis of the same flame as Fig. 1 (Flame 4, the ethylene/air flame). These images of soot aggregates are provided near the start of soot formation (Fig. 2a at z = 20 mm), near the maximum soot concentration condition (Fig. 2b at z = 50 mm) and near the end of soot surface oxidation (Fig. 2c at z = 70 mm).

The present soot particles were similar to soot observed during past studies within laminar premixed and diffusion flames, see Refs. 1-5, 7-9 and references cited therein, for other examples. The soot particles consisted of roughly spherical primary soot particles having nearly constant diameters at a given flame condition, as noted earlier. The primary particles were collected into open-structured aggregates that are known to be fractal aggregates based on earlier work, see Köylü and Faeth [33] and references cited therein. The aggregates had widely varying numbers of primary soot particles per aggregate with the average number of primary soot particles per aggregate progressively increasing with increasing distance from the burner exit. Present test conditions were limited to maximum amounts of soot oxidation (or cumulative levels of soot oxidation) of 70% by mass, based on the maximum primary particle diameter variation observed in each flame. Observations farther into the soot surface oxidation region yielded significantly reduced aggregate sizes as soot aggregates began to break up near the end of the soot surface oxidation process. It should also be noted that present levels of cumulative soot oxidation were smaller than conditions where Neoh et al. [23] observed effects of porous primary soot particles, internal oxidation of soot within primary particles, and soot aggregate breakup; therefore, oxidation of soot at the surface of primary soot particles dominated present observations.

Typical measurements of flame and soot properties along the axes of flames involving each fuel considered are illustrated in Figs. 3-7. In order to provide an example for each fuel for reference purposes, the results for an acetylene-nitrogen/air flame (Flame 1) illustrated in Fig. 3 were obtained from Xu and Faeth [7]. Similar results for the other fuels were obtained during the present investigation, as follows: the ethylene/air flame (Flame 4) illustrated in Fig. 4, the propylene-nitrogen/air flame (Flame 5) illustrated in Fig. 5, the propane/air flame (Flame 6) illustrated in Fig. 6, and an acetylene-benzene-nitrogen/air flame (Flame 8) illustrated in Fig. 7. Similar illustrations for the other two acetylene-nitrogen/air flames (Flames 2 and 3) can be found in Xu and Faeth [7] and Xu [8] whereas similar illustrations for the other two acetylene-benzene-nitrogen/air flames (Flames 7 and 9) can be found in El-Leathy [9]. Elapsed times of soot in the flames, found by integrating the velocity measurements, are indicated at the top of the plots; these times are relative to the first position where soot was observed at the measurement stations that were used (typically having 5 mm separation distances). Finally, in instances where the measurements extended beyond the flame sheet, the position of the flame sheet ($\phi=1$) is marked on the figures for reference purposes.

Gas (soot) temperatures in Figs. 3-7 reach a broad maximum in the soot formation region, somewhat before the flame sheet is reached. Thus, temperatures within the soot surface oxidation region either are roughly constant or decrease slightly with increasing distance from the burner exit. This behavior was observed for all the diffusion flames that were studied, e.g., Flames 1-9. As pointed out by Kent and Wagner [41,42] and Boedeker and Dobbs [43,44], and also observed during earlier laminar diffusion flame measurements in this laboratory [1-3,7], these reduced temperatures are caused by significant effects of continuum radiation heat losses from the present in soot-containing flames.

Gas velocities in Figs. 3-7 increase with increasing distance from the burner exit due to effects of buoyancy, e.g., velocities increase from burner exit values of 0.003-0.03 m/s to values in excess of 2 m/s at the highest position that was measured. This causes a corresponding stretching of the elapsed time scale at the top of the figures with increasing distance from the burner exit.

As discussed by Xu and Faeth [7], soot formation and oxidation proceed at the same time in diffusion flames and the boundary between the two regions is not abrupt. A reasonable definition of this boundary, mentioned earlier, is the point where the soot volume fraction reaches a maximum because soot formation and oxidation obviously dominate soot surface reaction processes before and after this condition, respectively. The results in Figs. 3-7 indicate that the boundary between the soot formation and oxidation regions generally is reached well before the flame sheet is reached, whereas the end of soot oxidation is reached either before or near the location of the flame sheet. Thus, the soot oxidation region generally involves small O_2 concentrations (less than 3% by volume) and is similar to conditions where Fenimore and Jones [19] and Mulcahy and Young [20] found that soot surface oxidation rates generally exceeded estimates based on the results of Nagle and Strickland-Constable [10]. For such conditions, they proposed that radicals such as O and OH might be strong contributors to the mechanism of soot surface oxidation.

For fuels other than acetylene, the original fuel disappears relatively close to the burner exit and concentrations of acetylene build up rapidly (benzene is an apparent exception but even benzene largely disappears near the burner exit, leaving a relatively small but nearly constant benzene concentration in the soot-containing region that only finally disappears near the flame sheet); as a result, concentrations of acetylene are rather similar for flames fueled with acetylene and with the other hydrocarbon fuels. Thus, similar to earlier observations of acetylene-fueled diffusion flames [1,7], the maximum soot volume fraction condition is reached when concentrations of acetylene become small (e.g., when acetylene mole fractions are smaller than 1%).

Results illustrated in Figs. 3-7 show that primary soot particle diameters reach a maximum relatively early in the soot formation region. This behavior occurs because soot growth maintains relatively rapid rates at temperatures smaller than those required for rapid rates of soot nucleation as noted by Tesner [45,46]; this behavior is discussed in earlier studies of soot processes in diffusion flames [1-3,7].

Concentrations of major stable gas species — N_2, CO_2 and H_2O — are seen to be relatively uniform in the soot surface oxidation region for the results illustrated in Figs. 3-7. This occurs for N_2 because its large concentration in the coflowing dry air causes it to dominate the flame composition. This behavior is also consistent with simple classical ideas about the structure of diffusion flames, where the concentrations of the stable combustion products — CO_2 and H_2O — should reach a maximum at the flame sheet. Also in agreement with classical ideas about the structure of diffusion flames, the concentrations of fuel-like species – C_2H_2, CO, H_2, CH_4, C_2H_4, C_2H_6, C_3H_6, C_3H_8 — all tend to decrease with increasing distance from the burner exit as fuel oxidation proceeds. Among the fuel species measured in the present flames, however, benzene is an exception. First of all, detectable concentrations of benzene could only be found in the flames fueled with benzene. Then, in the benzene-fueled flames, benzene decomposes from the burner exit similar to the other fuels but it subsequently reaches a small but nearly constant concentration (less than 1% by volume) throughout the fuel-rich region before finally disappearing near the flame sheet.

Concentrations of O_2 either progressively increase with increasing distance from the burner exit (Figs. 3 and 4) or progressively increase as the flame sheet is approached after reaching a broad minimum near the burner exit (Figs. 5-7). The latter behavior is probably caused by some leakage of coflowing O_2 into the fuel-rich region of the flames through the gap between the burner exit and the point where the flames are attached, similar to behavior observed for methane/air laminar coflowing jet diffusion flames by Mitchell et al. [47]. In addition, concentrations of fuel-like species, particularly H_2 and CO, penetrate well into the fuel-lean region. Thus, unlike approximations made during classical analysis of diffusion flames, effects of finite-rate chemistry, effects of dissociation, effects of preferential diffusion, and phenomena associated with the formation and oxidation of soot, cause fuel-like species to penetrate well into the fuel-lean region and oxidizer-like species to penetrate well into the fuel-rich region of the flames.

Concentrations of radical species illustrated in Figs. 3-7 are of interest due to the role that these species play in soot formation and oxidation. Measured concentrations of H, OH and O all increase with increasing distance from the burner exit (or as they approach the flame sheet). The measured radical concentrations were compared with equilibrium estimates of these concentrations found using the equilibrium data of Chase et al. [36] and present measurements of temperature and stable species concentrations. As a result of partial equilibrium requirements, superequilibrium ratios of H and OH are identical (Even the actual concentrations of these two radicals are not very different in the present flames, see Figs. 3-7). In addition, the variation of superequilibrium ratios along the axis of the flames was relatively independent of fuel type for present test conditions (in fact, the variation of radical concentrations themselves along the axis of the present flames is also qualitatively independent of fuel type, see Figs. 3-7). Near the start of soot formation (at z=10-20 mm), concentrations of H, OH and O are either near or somewhat below equilibrium levels. Subsequently, the superequilibrium ratios of all three radicals increase with increasing distance from the burner exit (or as the flame sheet is approached) with OH and H concentrations yielding superequilibrium ratios of 6-20 throughout most of the soot formation and oxidation regions. Notably, this tendency for the superequilibrium ratios of OH to reach values of this range while similarly increasing as the flame sheet is approached is very similar to the behavior seen in recent numerical predictions of the structure of soot-containing laminar coflowing jet diffusion flames involving methane/air and ethylene/air as reactants at atmospheric pressure due to McEnally et al. [48] and Smooke et al. [49]. Superequilibrium ratios of O are even larger than the rest, continuously increasing as the flame sheet is approached to reach values of 100-1000 near the downstream end of the soot-containing region (or the downstream end of the present measurements). The concentrations of H and OH, however, generally are significantly larger than concentrations of O throughout most of the soot formation and oxidation regions with concentrations of the three radicals only becoming comparable near the downstream end of the soot-containing region. This behavior differs substantially from the soot formation regions of premixed flames where the relatively slow variation of flame properties result in near-equilibrium levels of radical concentrations throughout [6]. Thus, the large superequilibrium concentrations of OH give rise to the possibility that soot surface oxidation in diffusion flames may be dominated by reaction with OH, as suggested by Fenimore and Jones [19], Mulcahy and Jones [19] and Neoh and coworkers [21-23], rather than by oxidation by O_2 and other potential oxidizing species. Notably, the numerical simulations of soot-containing laminar jet diffusion flames, involving methane/air and ethylene/air flames at atmospheric pressure, due to McEnally et al. [48] and Smooke et al. [49] also indicated that soot surface oxidation for these conditions was dominated by reaction with OH.

Soot Surface Oxidation Rate Measurements

Present measurements were exploited to study soot surface oxidation similar to earlier studies of soot growth [4,5,7]. Major assumptions were as follows: soot surface oxidation occurred only at the surface of primary soot particles, effects of thermophoresis and diffusion (Brownian motion) on soot motion are small so that soot particles convect at the local gas velocity, the soot density is constant, and the surface area available for soot surface oxidation is equivalent to constant diameter spherical soot particles that meet at a point. Present measurements were confined to the axis of the flames so that variations of soot properties as a function of time could be obtained directly from the elapsed time determinations illustrated in Figs. 3-7.

Properties that must be known to find soot surface oxidation rates include the number of primary particles per unit volume, n_p, the soot surface area per unit volume, S, and the mass of soot oxidized per unit soot surface area and time w_{ox}. The number of primary particles per unit volume was obtained from the measured soot volume fraction and primary particle diameter, as follows:

$$n_p = 6f_s/(\pi d_p^3) \tag{1}$$

with experimental uncertainties (95% confidence) of n_p estimated to be less than 32% for $f_s > 0.1$ ppm. The soot surface area per unit volume can be obtained from the same measured properties, as follows:

$$S = \pi d_p^2 n_p = 6f_s/d_p \tag{2}$$

where the last equality follows from Eq. 1; the experimental uncertainties (95% confidence) of S (which was found using the second formula of Eq. 2) are estimated to be less than 15% for $f_s >$ 0.1 ppm. Finally, conservation of soot mass along a streamline under the present assumptions yields an expression for the soot surface oxidation rate per unit surface area, w_{ox}, as follows:

$$w_{ox} = -(\rho/S)d(\rho_s f_s/\rho)dt \tag{3}$$

where S is found from Eq. 2 and the minus sign is inserted so that w_{ox} is a positive number. The gas density in Eq. 3 was found from measurements of gas species concentrations and temperatures, assuming an ideal gas mixture and neglecting the small volume of soot for present conditions (where soot concentrations were less than 2 ppm). The soot density in Eq. 3 was taken to be equal to 1850 kg/m^3, similar to past work [1-5,7]. The temporal derivatives in Eq. 3 were found from three-point least-squares fits of the argument of the derivative, $\rho_s f_s/\rho$, which also is similar to past work [1-5,7].

Present measurements of soot surface oxidation rates were corrected for effects of soot surface growth based on the Hydrogen-Abstraction/Carbon-Addition (HACA) soot surface growth rate mechanism of Colket and Hall [50]. In particular, this soot surface growth rate mechanism has provided successful correlations of measured soot surface growth rates in both premixed and diffusion flames [4,5] and diffusion flames [7,9], including all the diffusion flames considered during the present study of soot surface oxidation rates in laminar diffusion flame environments. No condition is considered in the following, however, where the correction for effects of the soot surface growth rate was more than half the soot surface oxidation rate, in order to minimize effects of current uncertainties about soot surface growth rates on soot surface oxidation rates.

Similar to Neoh et al. [21,22], present soot surface oxidation rates (corrected for effects of soot surface growth rates) were converted into collision efficiencies (or reaction probabilities) based on kinetic theory estimates of the collision rates of a given gas species with the surfaces of primary soot particles. Thus, the collision efficiency, η_i, for a potential oxidizing species, i, is given by the following expression [2]:

$$\eta_i = 4w_{ox}/(C_i[i]\,\bar{v}_i) \tag{4}$$

where C_i is the mass of carbon removed from the surface per mole of species i reacting at the surface, [i] is the gas phase concentration of i adjacent to the surface, and

$$\bar{v}_i = (8R_uT/(\pi M_i))^{1/2} \tag{5}$$

is the (Boltzmann) equilibrium mean molecular velocity of species i. In the following, values of the η_i will be considered for potential soot surface oxidation by O_2, CO_2, H_2O, O and OH, in turn.

Similar to past studies of soot surface oxidation due to Neoh et al. [21-23], Garo et al. [27,28], Puri et al. [29,30] and Haudiquert et al. [31], two limiting approaches were taken to consider the potential effect of soot surface oxidation by the O_2 that was present at all our test conditions, as follows: (1) soot surface oxidation by the species under consideration was assumed to only occur by the collisional mechanism of Eqs. 4 and 5 alone, and (2) the collisional mechanism was assumed to occur in parallel with an existing empirical soot surface oxidation mechanism involving O_2 that was in the literature, e.g., the O_2 soot surface oxidation rate formulas of Nagle and Strickland-Constable [10] and Lee et al. [51]. The past studies of Neoh and coworkers [21-23], Garo et al. [27,28], and Haudiquert et al. [31] all used the widely recognized empirical O_2 soot surface oxidation rate formulas of Nagle and Strickland-Constable [10], whereas Haudiquert et al. [31] considered the expression of Lee et al. [51] as well; in all cases, it was found that effects of direct oxidation rates estimated from Refs. 10 and 51 were small for the O_2 concentrations present for the various test conditions (which generally were smaller than 5% by volume). Present test conditions were similar in this respect with O_2 concentrations smaller than 3% by volume in the region where soot surface oxidation rates were measured; therefore, corrections of present soot surface oxidation rates using the O_2 rate expression of Nagle and Strickland-Constable [10] were small. Puri et al. [29], however, point out that the Nagle and Strickland-Constable [10] expression is subject to some uncertainty based on the measurements of Levendis et al. [52], Chan et al. [53], Felder et al. [54] and Cadman et al. [55]. Present measurements of soot surface oxidation rates are limited to the temperature range of 1700-1800 K, where the Nagle and Strickland-Constable [10] estimates of soot surface oxidation rates by O_2 are in reasonably good agreement with the measurements of Park and Appleton [14] and Levendis et al. [52]. The Chan et al. [53] O_2 surface oxidation rates are significantly smaller than the Nagle and Strickland-Constable [10] rates but their measurements are limited to temperatures of 770-1250 K, which is well below the range of present interest. Similarly, Felder et al. [54] find soot surface oxidation rates by O_2 significantly smaller than estimates from Nagle and Strickland-Constable [10] and speculate that this behavior might be due to the presence of sulfur as an impurity in their carbon black samples; this difficulty clearly is not a problem for the soot aggregates studied during the present investigation. In contrast to the rest, Cadman et al. [55] report soot surface oxidation rates due to O_2 that are roughly six times larger than estimates from Nagle and Strickland-Constable [10] for the temperature range of interest for the present study. On balance, however, it appears that the Nagle and Strickland-Constable [10] predictions of soot surface oxidation rates by O_2 generally overestimate these rates and since the effect of direct soot surface oxidation was small for conditions of interest here serves as a widely recognized estimate of this effect for present purposes.

The collision efficiencies of O_2 for soot surface oxidation are plotted as a function of height above the burner in Fig. 8. Results shown on the figure include the range of values observed by Neoh et al. [21,22] in premixed flames, the values determined from the present experiments in diffusion flames, and values estimated from the predictions of Nagle and Strickland-Constable [10] for the conditions where present observations were made in diffusion flames. As just discussed, the Nagle and Strickland-Constable [10] approach has exhibited effective capabilities to predict soot surface oxidation by O_2 and there are significant levels of O_2 along the present soot paths, see Figs. 3-7. Thus, the fact that the Nagle and Strickland-Constable estimates of the O_2 collision efficiency are 10-100 times smaller than the present measurements strongly suggests that some other species is mainly responsible for soot surface oxidation in the present flames. Other evidence that O_2 is not the main direct soot oxidizing species for flame environments is provided by the large scatter (nearly a factor of 100) of the present collision efficiencies for diffusion flames combined with the even larger scatter (more than a factor of 100) of the O_2 collision efficiencies of Neoh et al. [21] in premixed flames.

The collision efficiencies of CO_2 for soot surface oxidation are plotted as a function of height above the burner in Fig. 9. Results shown on the figure include the range of values observed by Neoh et al. [21] in premixed flames, and values from the present investigation in diffusion flames both considering and ignoring the contribution of oxidation by O_2 (estimated using the Nagle and Strickland-Constable [10] correlation). First of all, it is evident that allowing for direct soot surface oxidation by O_2 generally only has a small effect on the collision efficiencies estimated in Fig. 9. In addition, there is significant scatter (more than a factor of 10) of the present collision efficiencies for diffusion flames and even larger scatter (nearly a factor of 100) of the collision efficiencies of Neoh et al. [21] in premixed flames. These findings clearly do not support CO_2 as a major direct contributor to soot surface oxidation in flame environments either alone or in parallel with soot surface oxidation by O_2.

The collision efficiencies of H_2O for soot surface oxidation are plotted as a function of height above the burner in Fig. 10, in the same manner as the results for CO_2 surface oxidation of soot in Fig. 9. The observations are the same: O_2 surface oxidation makes only a minor contribution to soot surface oxidation in parallel with H_2O and H_2O collision efficiencies exhibit large scatter (nearly a factor of 100) in both premixed and diffusion flames. These findings also clearly do not support H_2O as a major direct contributor to soot surface oxidation in flame environments either alone or in parallel with soot surface oxidation by O_2.

The collision efficiencies of O for soot surface oxidation are plotted as a function of height above the burner in Fig. 11, in the same manner as the results for CO_2 and H_2O surface oxidation of soot in Figs. 9 and 10. The results are much the same: direct O_2 surface oxidation is not very important and collision efficiencies of O exhibit large scatter (more than a factor of 10) in both premixed and diffusion flames. In addition, relatively small concentrations of O compared to other potential oxidizing species in both the premixed and diffusion flames would require unrealistic collision efficiencies greater than unity if O was the major soot surface oxidizing species for the results illustrated in Fig. 11. These findings also clearly do not support O as a major direct contributor to soot surface oxidation in flame environments.

Finally, the collision efficiencies of OH for soot surface oxidation are plotted as a function of height above the burner in Fig. 12, in the same manner as the results for CO_2 and H_2O and O surface oxidation of soot in Figs. 9-11. With perhaps one exception, direct O_2 surface oxidation of soot is not very important for these conditions, as before. On the other hand, similar to the observations of Neoh et al. [21], present collision efficiencies of OH exhibit relatively small levels of scatter (roughly a factor of 3), compared to the other potential soot oxidizing species that have been considered. Furthermore, the results for premixed and diffusion flames in Fig. 12 are in remarkably good agreement with each other. In particular, the collision efficiency of OH for soot surface oxidation in the present diffusion flames is 0.14 with an uncertainty (95% confidence) of ± 0.04 after allowing for direct soot surface oxidation by O_2 using estimates from Nagle and Strickland-Constable [10]; this is in excellent agreement with the value for soot surface oxidation from Neoh et al. [21] in premixed flames of 0.13 with an uncertainty (95% confidence) of ± 0.03 when using the same treatment of soot structure and is in fair agreement with measurements of Garo et al. [27,28] and Haudiquert et al. [31] as discussed earlier, all of which corrected for direct soot surface oxidation by O_2 using the results of Ref. 10. In addition, the effects of the fuel type used also has only a modest effect on the soot surface oxidation by OH for the range of present test conditions. Finally, direct effects of soot surface oxidation were modest for present test conditions, with the OH collision efficiency increasing from 0.14 to 0.17 when direct soot surface oxidation by O_2 was ignored. This behavior was achieved over a relatively broad range of flame conditions for the combined results in premixed and diffusion flames, as follows: temperatures of 1570-1870 K, oxygen mole fractions of $1 \times 10^{-5} - 3 \times 10^{-2}$ and levels of soot mass consumption less than 70% at atmospheric pressure. While these results are helpful, however, the properties of the final stage of oxidation, where internal oxidation of primary particles becomes a factor, effects of pressure on soot surface oxidation, effects of higher temperatures (> 2000 K, say, which are of interest for many practical applications) and additional consideration of fuel type, e.g., fuels containing oxygen would be of interest due to their potential to increase OH concentrations in the soot oxidation zone, see Bennett et al. [56], all merit additional study in the future.

CONCLUSIONS

Flame structure and soot surface oxidation processes were studied in the soot surface oxidation region of coflowing laminar jet diffusion flames. Test conditions involved acetylene-nitrogen, ethylene-, propylene-nitrogen, propane and acetylene-benzene fuel mixtures burning in air at atmospheric pressure as summarized in Table 1. For these flames, O_2 mole fractions were generally smaller than 3% in the region where soot surface oxidation was observed. The major conclusions of the study are as follows:

1. Potential soot surface oxidizing species in the region that was studied include O_2, CO_2, H_2O, O and OH. The radicals OH and H exhibited superequilibrium concentrations by factors as large as 10-20. The radical O exhibited even larger superequilibrium ratios, up to 1000, but absolute concentrations of O were generally significantly smaller than concentrations of OH and H. Among these species, OH was mainly responsible for soot surface oxidation with significant levels of soot surface oxidation beginning at fuel-rich conditions.

2. Present soot surface oxidation rates could be correlated by assuming a constant collision efficiency of OH of 0.14 with an uncertainty (95% confidence) of ± 0.04 after allowing for direct O_2 soot surface oxidation based on estimates from Nagle and Strickland-Constable

[10], and with no significant effect of fuel type observed for this behavior. This finding is in good agreement with the OH collision efficiency for soot surface oxidation of soot of 0.13 with an uncertainty (95% confidence) of ± 0.03 for assumed similar soot structure properties found by Neoh et al. [21] from measurements in premixed flames at similar O_2 concentrations and atmospheric pressure, and are in fair agreement with earlier measurements of soot surfrace oxidation due to OH in diffusion flames at atmospheric pressure reported by Garo et al. [27,28] and Haudiquert et al. [31].

3. The correction of present soot surface oxidation rates for oxidation by O_2 based on the results of Nagle and Strickland-Constable [10] was small, (e.g., the collision efficiency for OH increased from 0.14 to 0.17 when soot surface oxidation by O_2 was ignored) compared to oxidation by OH for present conditions. Soot surface oxidation at leaner conditions, particularly when temperatures are elevated, should exhibit a larger contribution from O_2; this transition has received little attention, however, and merits additional study in the future. Other issues concerning soot surface oxidation that merit attention in the future include effects of internal oxidation in the final stages of oxidation, effects of pressure, effects of relatively high temperatures (greater than 2000 K) and additional study of effects of fuel type (especially oxygen-containing fuels that should increase OH concentrations at fuel-rich conditions [56]).

This research was sponsored by NASA grants NCC3-661, NAG-3-1878, NAG-3-2048 and NAG3-2404 under the technical management of D. L. Urban and Z.-G. Yuan of the NASA Glenn Research Center.

REFERENCES

1. Sunderland, P.B., Köylü, Ü.Ö., and Faeth, G.M., Combust. Flame 100:310 (1995).

2. Sunderland, P.B., and Faeth, G.M., Combust. Flame 105:132 (1996).

3. Lin, K.-C., Sunderland, P.B., and Faeth, G.M., Combust. Flame 104:375 (1996).

4. Xu, F., Sunderland, P.B., and Faeth, G.M., Combust. Flame 108:471 (1997).

5. Xu, F., Lin, K.-C., and Faeth, G.M., Combust. Flame 115:195 (1998).

6. Xu, F., and Faeth, G.M., Combust. Flame 121:640 (2000).

7. Xu, F., and Faeth, G.M., Combust. Flame 125:804 (2001).

8. Xu, F., *Soot Growth in Laminar Premixed Flames*, Ph.D. Thesis, The University of Michigan, 1999.

9. El-Leathy, A.M., *Effects of Fuel Type on Soot Formation and Oxidation in Laminar Diffusion Flames*, Ph.D. Thesis, Helwan University , Cairo, Egypt, 2002.

10. Nagle, J., and Strickland-Constable, R.F., *Proceedings of Fifth Carbon Conference* 1:154 (1962).

11. Rosner, D.E., and Allendorf, H.D., AIAA J. 6:650 (1968).

12. Wright, F.J., Proc. Combust. Inst. 15:1449 (1974).

13. Radcliffe, S.W., and Appleton, J.P., Combust. Sci. Tech. 4:171 (1971).

14. Park, C., and Appleton, J.P., Combust. Flame 20:369 (1973).

15. Libby, P.A., and Blake, T.R., Combust. Flame 36:139 (1979).

16. Libby, P.A., and Blake, T.R., Combust. Flame 41:123 (1981).

17. Johnstone, J.F., Chen, C.Y., and Scott, D.S., Ind. Engr. Chem. 44:1564 (1952).

18. Bradley, D., Dixon-Lewis, G., El-Din Habik, S., and Mushi, E.M.J., Proc. Combust. Inst. 20:931 (1984).

19. Fenimore, C.P., and Jones, C.W., J. Phys. Chem. 71:593 (1967).

20. Mulcahy, M.F.R., and Young, B.C., Carbon 13:115 (1975).

21. Neoh, K.G., Howard, J.B., and Sarofim, A.F., *Particulate Carbon* (D.C. Siegla and B.W. Smith, ed.), Plenum Press, New York, 1980, p. 261.

22. Neoh, K.G., *Soot Burnout in Flames*, Ph.D. Thesis, Massachusetts Institute of Technology, Cambridge, MA, 1980.

23. Neoh, K.G., Howard, J.B., and Sarofim, A.F., Proc. Combust. Inst. 20:951 (1984).

24. Wicke, B.C., Wong, C., and Grady, K.A., Combust. Flame 66:37 (1986).

25. Wicke, B.C., and Grady, K.A., Combust. Flame 69:185 (1987).

26. Roth, P., Brandt, O., and von Gersum, S., Proc. Combust. Inst. 23:1485 (1990).

27. Garo, A., Lahaye, J., and Prado, G., Proc.Combust. Inst. 21:1023 (1986).

28. Garo, A., Prado, G., and Lahaye, J., Combust. Flame 79:226 (1990).

29. Puri, R., Santoro, R.J., and Smyth, K.C., Combust. Flame 97:125 (1994).

30. Puri, R., Santoro, R.J., and Smyth, K.C., Combust. Flame 102:226 (1995).

31. Haudiquert, M., Cessou, A., Stepowski, D., and Coppalle, A., Combust. Flame 111:338 (1997).

32. Wersborg, B.L., Howard, J.B., and Williams, G.C., Proc. Combust. Inst. 14:929 (1972).

33. Köylü, Ü.Ö., and Faeth, G.M., J. Heat Trans. 115:409 (1993).

34. Dalzell, W.H., and Sarofim, A.F., J. Heat Trans. 91:100 (1969).

35. Krishnan, S.S., Lin, K.-C., and Faeth, G.M., J. Heat Trans. 122:517 (2000).

36. Chase, M.W., Jr. Davies, C.A., Downey, J.R., Jr., Frurip, D.J., McDonald, R.R., and Syverud, A.N., *JANAF Thermochemical Tables*, 3rd ed., J. Phys. Chem. Ref. Data 14 (Supplement 1): 1211 (1986).

37. McBride, B.J., Reno, M.A., and Gordon, S., *CET93 and CETPC: An Interim Updated Version of the NASA Lewis Computer Program for Calculating Complex Chemical Equilibrium with Applications*, NASA Technical Memorandum 4557, Washington, D.C., 1994.

38. Hamins, A., Gordon, A.S., Saito, K., and Seshadri, K., Combust. Sci. Tech. 45:309 (1986).

39. Colket, M.B, III, Seery, D.J., and Palmer, H.B., Combust. Flame 75:343 (1989).

40. Colket, M.B, III, Seery, D.J., and Palmer, H.B., Combust. Flame 84:434 (1991).

41. Kent, J. H., and Wagner, H. Gg., Proc.Combust. Inst. 20:1007 (1984).

42. Kent, J.H., and Wagner, H.Gg., Combust. Sci. Tech. 41:245 (1984).

43. Boedecker, L.R., and Dobbs, G.M., Proc. Combust. Inst. 21:1097 (1986).

44. Boedecker, L.R., and Dobbs, G.M., Combust. Sci. Tech. 46:301 (1986).

45. Tesner, P.A., Proc. Combust. Inst. 7:536 (1958).

46. Tesner, P.A., Proc. Combust. Inst. 8:627 (1960).

47. Mitchell, R.E., Sarofim, A.F., and Clomberg, L.A., Combust. Flame 37:227 (1980).

48. McEnally, C.S., Schaffer, A.M., Long, M.B., Pfefferle, L.D., Smooke, M.D., Colket, M.B., and Hall, R.J., Proc. Combust. Inst. 27:1497 (1998).

49. Smooke, M.D., McEnally, C.S., Pfefferle, L.D., Hall, D.J., and Colket, M.B., Combust. Flame 117:117 (1999).

50. Colket, M.B., and Hall, R.J., in *Soot Formation in Combustion* (H. Bockhorn, ed.), Springer-Verlag, Berlin, 1994, p. 442.

51. Lee, K.B., Thring, M.W., and Beer, J.M., Combust. Flame 6:137 (1962).

52. Levendis, Y.A., Flagan, R.C., and Gavalas, G.R., Combust. Flame 76:221 (1989).

53. Chan, M.-L., Moody, K.N., Mullins, J.R., and Williams, A., Fuel 66:1694 (1987).

54. Felder, W., Madronich, S., and Olson, D.B., Energy and Fuels 2:743 (1988).

55. Cadman, P., Cornish, R., and Denning, R.J., 17th International Shock Tube Symposium, American Institute of Physics, 1990, p. 751.

56. Bennett, B.A.V., McEnally, C.S., Pfefferle, L.D., and Smooke, M.D., Combust. Flame 123:522 (2000).

Table 1 Summary of the test laminar jet diffusion flames[a]

Flame	1	2	3	4	5	6	7	8	9
Fuel	C_2H_2	C_2H_2	C_2H_2	C_2H_4	C_3H_6	C_3H_8	C_6H_6	C_6H_6	C_6H_6
Fuel in fuel stream (% by vol.)	16.9	15.1	17.3	100.0	18.8	100.0	0.6	1.3	2.2
C_2H_2 in fuel stream (% by vol.)[b]	---	---	---	---	---	---	14.0	10.2	5.5
N_2 in fuel stream (% by vol.)	83.1	84.9	82.7	---	81.2	---	85.4	88.5	92.3
Fuel stream flow (cc/s)[c]	26.10	22.90	31.30	5.52	16.62	3.20	28.92	29.37	30.02
Dry air coflow (cc/s)[c]	94.7	94.7	94.7	292.0	222.0	222.0	160.0	160.0	160.0
Burner exit velocity (mm/s)[d]	27.4	31.4	32.4	5.8	17.4	3.4	30.4	30.9	31.6
Dry air coflow velocity (mm/s)[d]	56.0	56.0	56.0	171.0	130.0	130.0	94.0	94.0	94.0
Luminous flame length (mm)	82	80	103	100	100	100	90	90	90
Stoich. flame length (mm)	100	106	116	81	74	79	95	130	110
Re (-)	62	71	74	23	92	25	74	76	78
$Fr \times 10^5$ (-)	220	290	310	10	89	3	270	280	290
Stoich. flame temperature (K)	2380	2320	2390	2370	2150	2260	2140	2050	1900

---

[a] Laminar round coflowing jet diffusion flames with a 38.4 mm inside diameter fuel stream port and a 60 mm inside diameter concentric dry air port, both directed vertically upward. Ambient temperature and pressure of 294 ± 2 K and 98 ± 1 kPa. Gas purities (% by vol.) as follows: N_2=99.9%; O_2=99.6%; C_2H_2=99.6%; C_2H_4=99.5%; C_3H_6=99.5%; dry air coflow of 79% N_2 and 21% O_2 by vol.

[b] Unless acetylene is the fuel in which case the concentration of acetylene in the fuel stream is given by the % by vol. of the fuel in the fuel stream.

[c] Volume flow rate based on standard conditions of 300 K and 101.3 kPa.

[d] Adiabatic flame temperature for stoichiometric combustion of the fuel stream in dry air with the reactants at 300 K and combustion at 101.3 kPa.

List of Figures

Fig. 1 Dark-field photograph of a typical laminar jet diffusion flame: the ethylene-fueled flame burning in air at atmospheric pressure (Flame 4, fuel stream of 100% C_2H_4 by volume).

Fig. 2 Typical TEM photographs of soot aggregates along the axis of the ethylene-fueled laminar jet diffusion flame burning in air at atmospheric pressure (Flame 4, fuel stream of 100% C_2H_4 by volume): 2a. photograph near start of soot formation ($z = 20$ mm), 2b. photograph near the maximum soot concentration condition ($z = 50$ mm); 2c. photograph near the end of soot surface oxidization ($z = 70$ mm).

Fig. 3 Measured soot and flame properties along the axis of an acetylene-nitrogen/air laminar jet diffusion flame at atmospheric pressure (Flame 1, fuel stream of 16.9% C_2H_2 and 83.1% N_2 by volume, from Xu and Faeth [7]).

Fig. 4 Measured soot and flame properties along the axis of an ethylene/air air laminar jet diffusion flame at atmospheric pressure (Flame 4, fuel stream of 100% C_2H_4 by volume).

Fig. 5 Measured soot and flame properties along the axis of a propylene-nitrogen/air laminar jet diffusion flame at atmospheric pressure (Flame 5, fuel stream of 18.8% C_3H_6 and 81.2% N_2 by volume).

Fig. 6 Measured soot and flame properties along the axis of a propane/air laminar jet diffusion flame at atmospheric pressure (Flame 6, fuel stream of 100% C_3H_8 by volume).

Fig. 7 Measured soot and flame properties along the axis of an acetylene-benzene-nitrogen/air laminar jet diffusion flame at atmospheric pressure (Flame 8, fuel stream of 10.2% C_2H_2, 1.3% C_6H_6 and 88.5% N_2 by volume).

Fig. 8 Collision efficiencies assuming soot burnout due to attack by O_2 as a function of height above the burner. Found from the measurements of Neoh et al. [21] in premixed flames, estimated from the predictions of Nagle and Strickland-Constable [10] for the conditions of the present diffusion flames, and found from present measurements in diffusion flames.

Fig. 9 Collision efficiencies assuming soot burnout due to attack by CO_2 as a function of height above the burner. Found from the measurements of Neoh et al. [21] in premixed flames, and from the present measurements in diffusion flames with and without parallel O_2 attack estimated from the predictions of Nagle and Strickland-Constable [10].

Fig. 10 Collision efficiencies assuming soot burnout due to attack by H_2O as a function of height above the burner. Found from the measurements of Neoh et al. [21] in premixed flames, and from the present measurements in diffusion flames with and without parallel O_2 attack estimated from the predictions of Nagle and Strickland-Constable [10].

Fig. 11 Collision efficiencies assuming soot burnout due to attack by O as a function of height above the burner. Found from the measurements of Neoh et al. [21] in premixed flames, and from the present measurements in diffusion flames with and without parallel O_2 attack estimated from the predictions of Nagle and Strickland-Constable [10].

Fig. 12 Collision efficiencies assuming soot burnout due to attack by OH as a function of height above the burner. Found from the measurements of Neoh et al. [21] in premixed flames, and from the present measurements in diffusion flames with and without parallel O_2 attack estimated from the predictions of Nagle and Strickland-Constable [10].

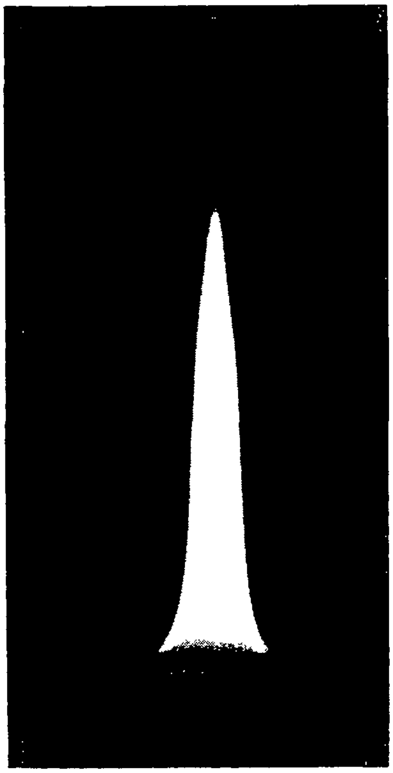

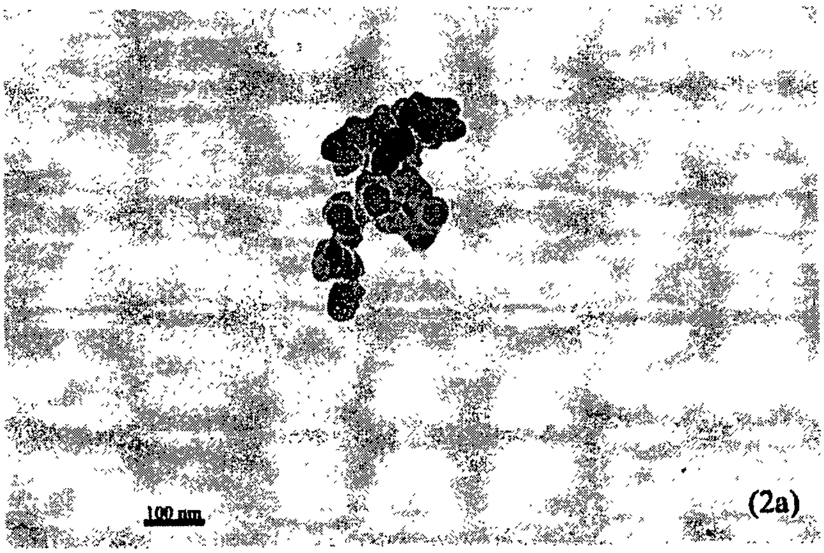

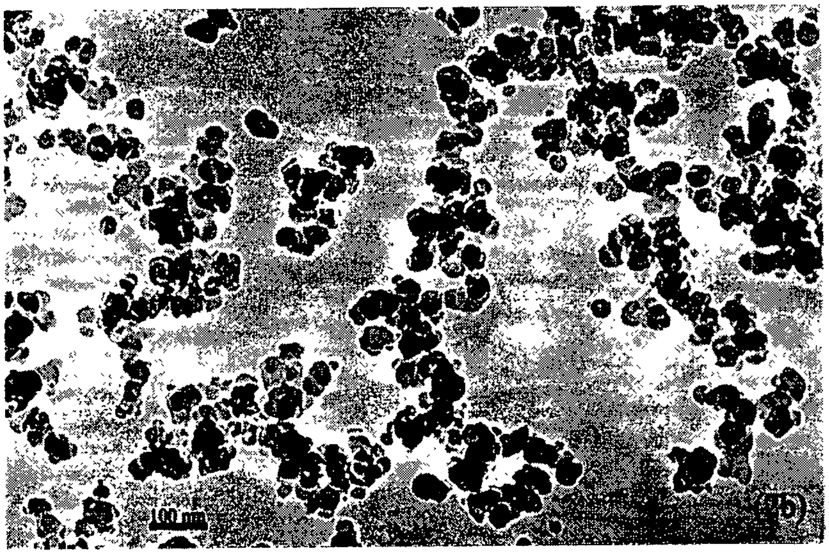

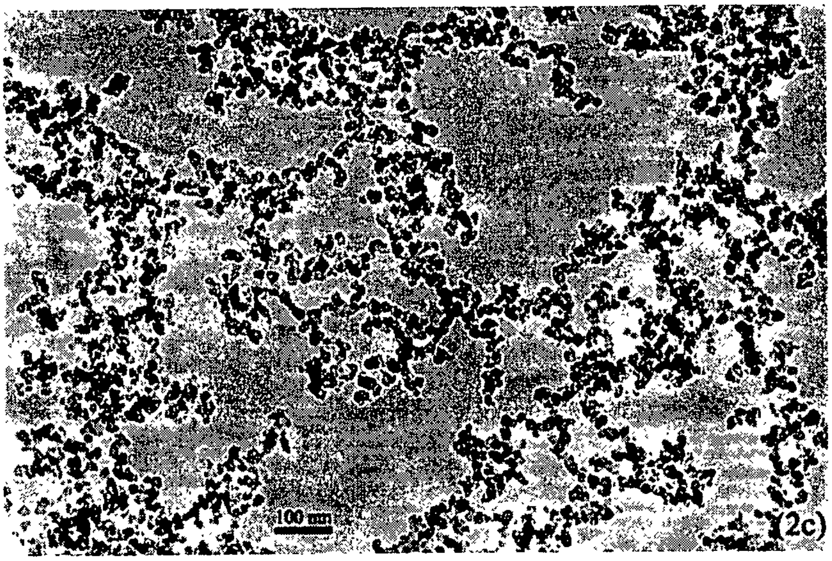

②

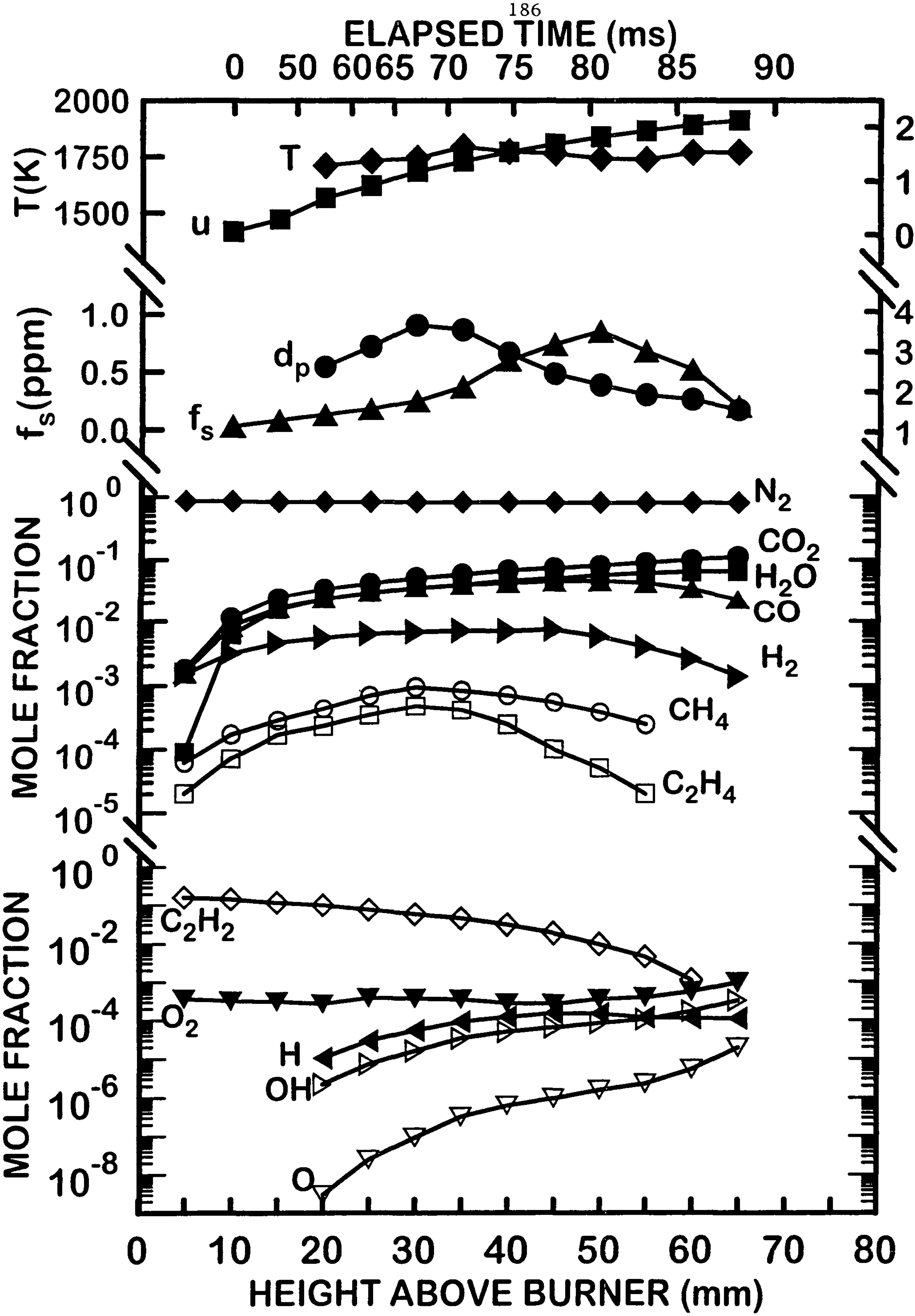
ELAPSED TIME (ms)
0
50
60
65
70
75
80
85
90
T(K)
2000
1750
1500
u (m/s)
2.0
1.0
0.0
T
u
f_s (ppm)
1.0
0.5
0.0
d_p (nm)
40
30
20
10
d_p
f_s
MOLE FRACTION
10^0
10^-1
10^-2
10^-3
10^-4
10^-5
N_2
CO_2
H_2O
CO
H_2
CH_4
C_2H_4
MOLE FRACTION
10^0
10^-2
10^-4
10^-6
10^-8
C_2H_2
O_2
H
OH
O
0
10
20
30
40
50
60
70
80
HEIGHT ABOVE BURNER (mm)

③

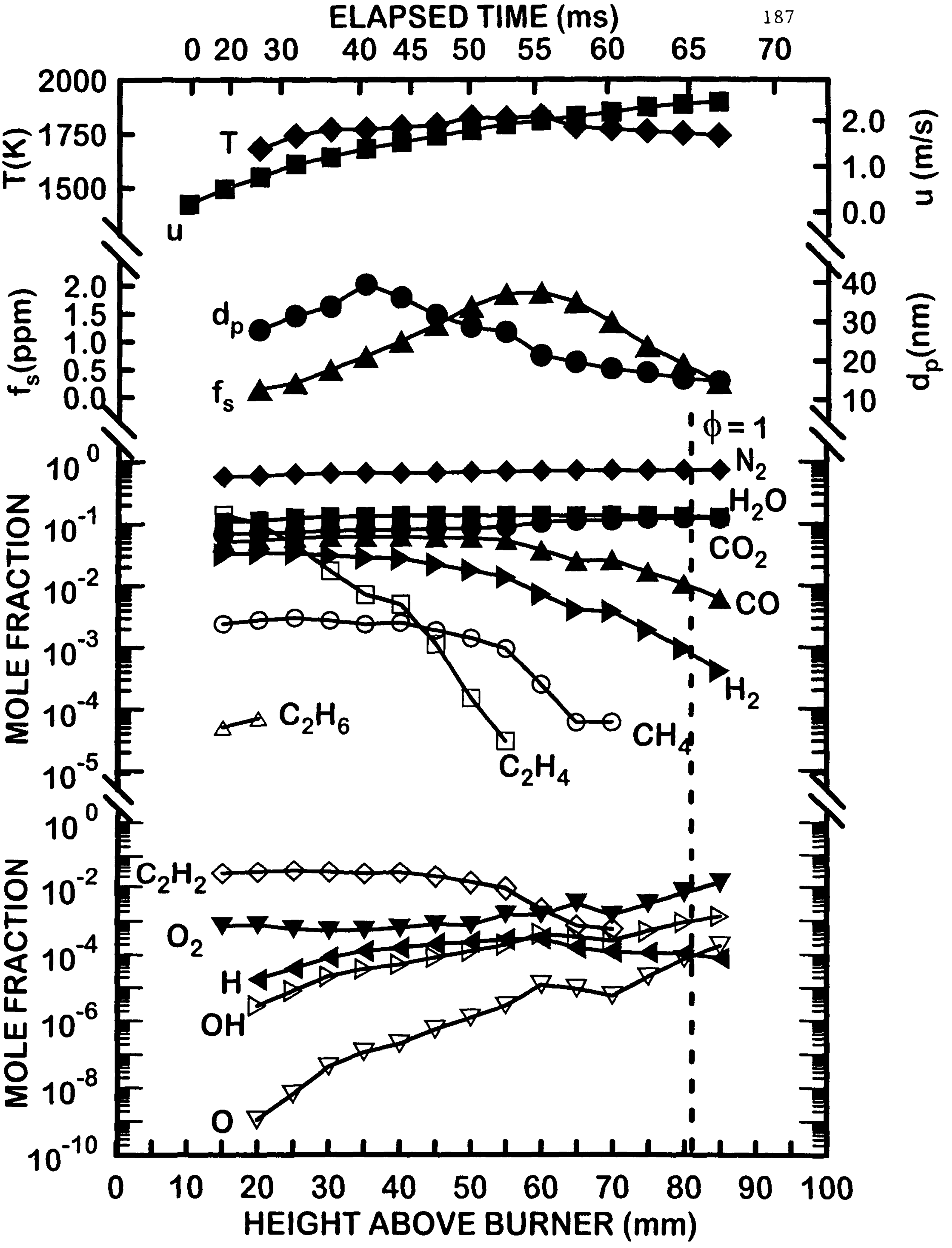
ELAPSED TIME (ms)
0 20 30 40 45 50 55 60 65 70
T(K)
2000
1750
1500
u (m/s)
2.0
1.0
0.0
T
u
f_s(ppm)
2.0
1.5
1.0
0.5
0.0
d_p(nm)
40
30
20
10
d_p
f_s
$\phi = 1$
MOLE FRACTION
10^0
10^{-1}
10^{-2}
10^{-3}
10^{-4}
10^{-5}
N_2
H_2O
CO_2
CO
H_2
CH_4
C_2H_4
C_2H_6
MOLE FRACTION
10^0
10^{-2}
10^{-4}
10^{-6}
10^{-8}
10^{-10}
C_2H_2
O_2
H
OH
O
0 10 20 30 40 50 60 70 80 90 100
HEIGHT ABOVE BURNER (mm)

④

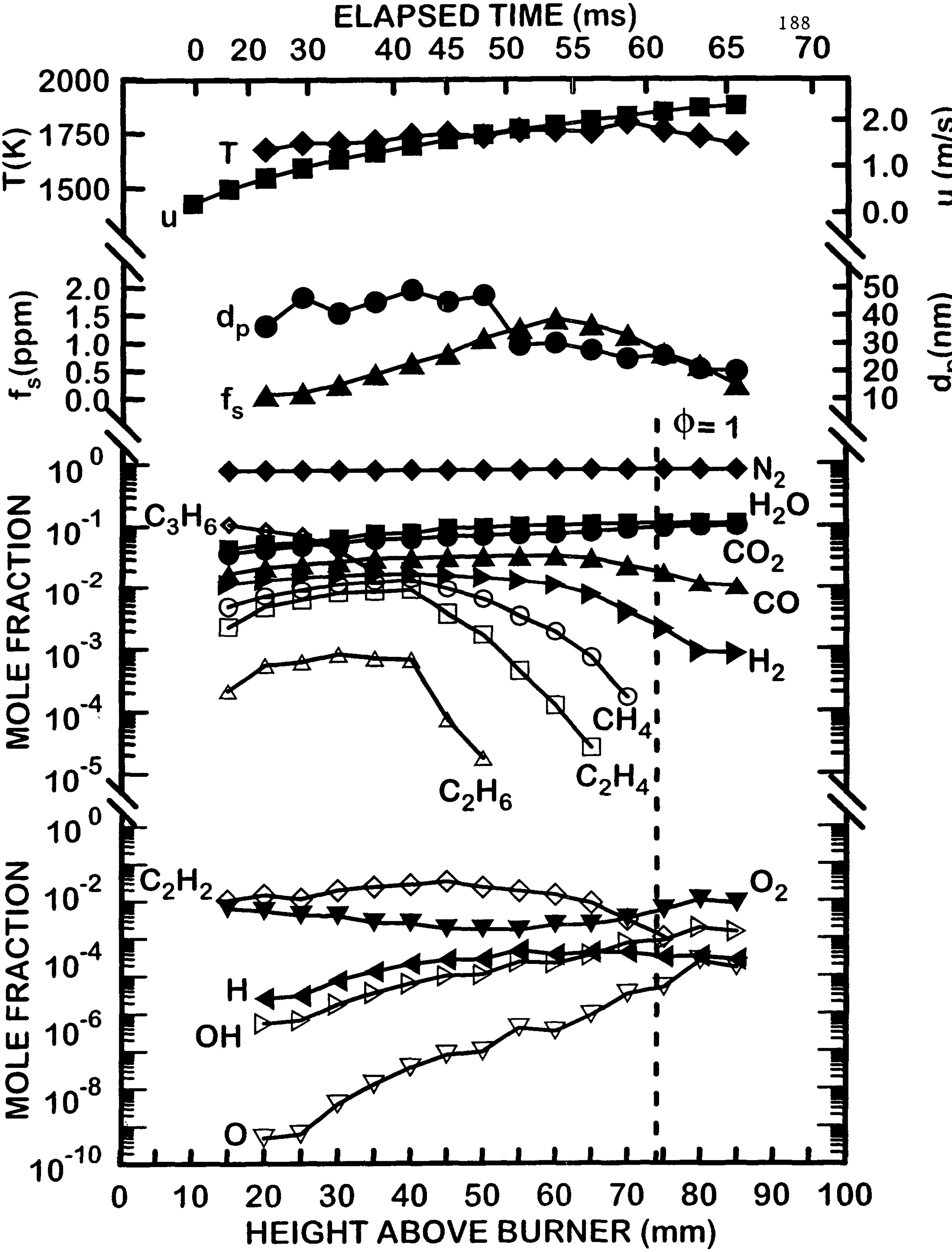
ELAPSED TIME (ms)
0
20
30
40
45
50
55
60
65
70
T(K)
2000
1750
1500
T
u
2.0
1.0
0.0
u (m/s)
f_s(ppm)
2.0
1.5
1.0
0.5
0.0
d_p
f_s
50
40
30
20
10
d_p(nm)
ϕ= 1
MOLE FRACTION
10^0
10^{-1}
10^{-2}
10^{-3}
10^{-4}
10^{-5}
N_2
C_3H_6
H_2O
CO_2
CO
H_2
CH_4
C_2H_4
C_2H_6
MOLE FRACTION
10^0
10^{-2}
10^{-4}
10^{-6}
10^{-8}
10^{-10}
C_2H_2
O_2
H
OH
O
0
10
20
30
40
50
60
70
80
90
100
HEIGHT ABOVE BURNER (mm)

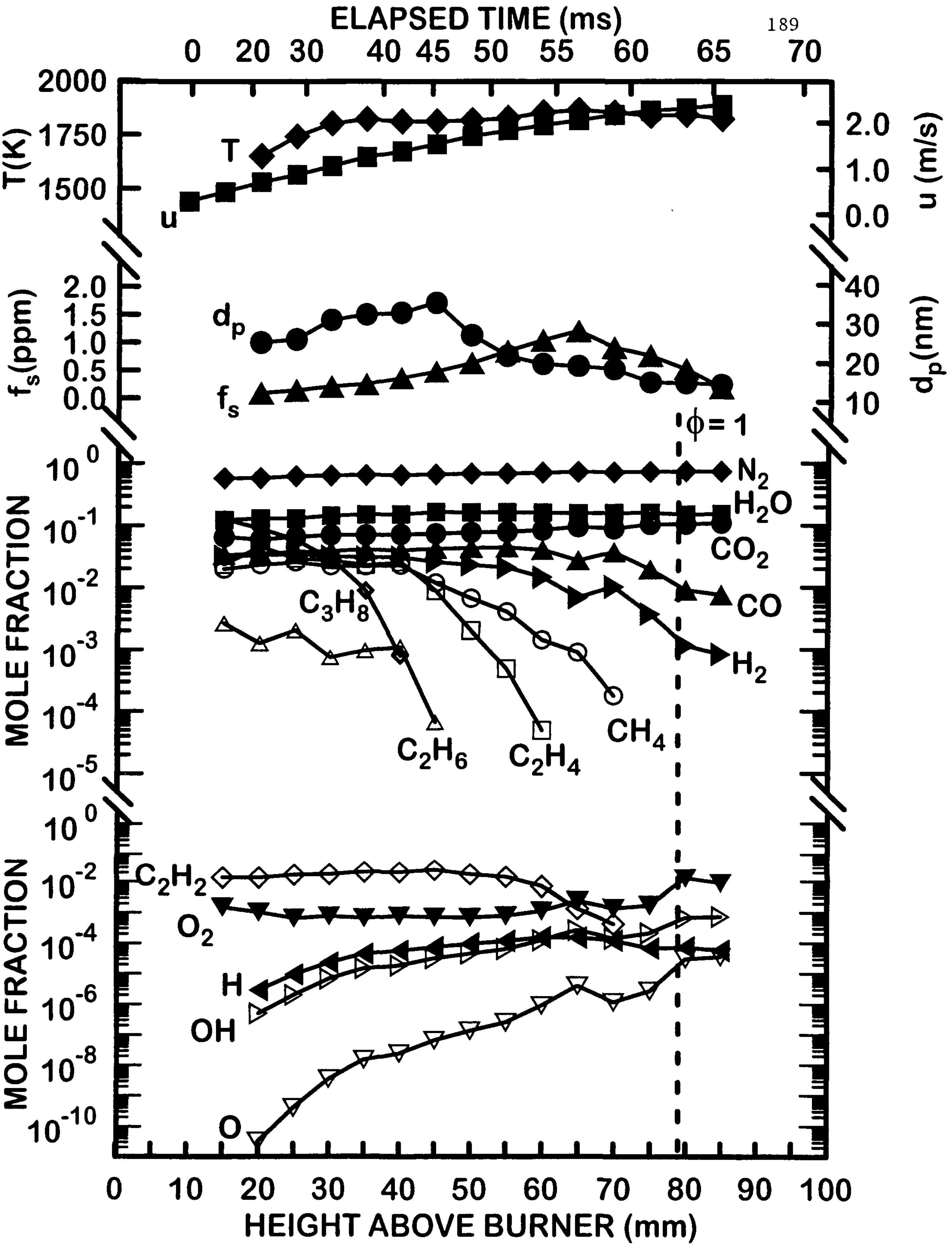
ELAPSED TIME (ms)
0
20
30
40
45
50
55
60
65
70
T(K)
2000
1750
1500
T
u
u (m/s)
2.0
1.0
0.0
f_s(ppm)
2.0
1.5
1.0
0.5
0.0
d_p
f_s
d_p(nm)
40
30
20
10
$\phi = 1$
MOLE FRACTION
10^0
10^{-1}
10^{-2}
10^{-3}
10^{-4}
10^{-5}
N_2
H_2O
CO_2
CO
H_2
C_3H_8
C_2H_6
C_2H_4
CH_4
MOLE FRACTION
10^0
10^{-2}
10^{-4}
10^{-6}
10^{-8}
10^{-10}
C_2H_2
O_2
H
OH
O
0
10
20
30
40
50
60
70
80
90
100
HEIGHT ABOVE BURNER (mm)

⑥

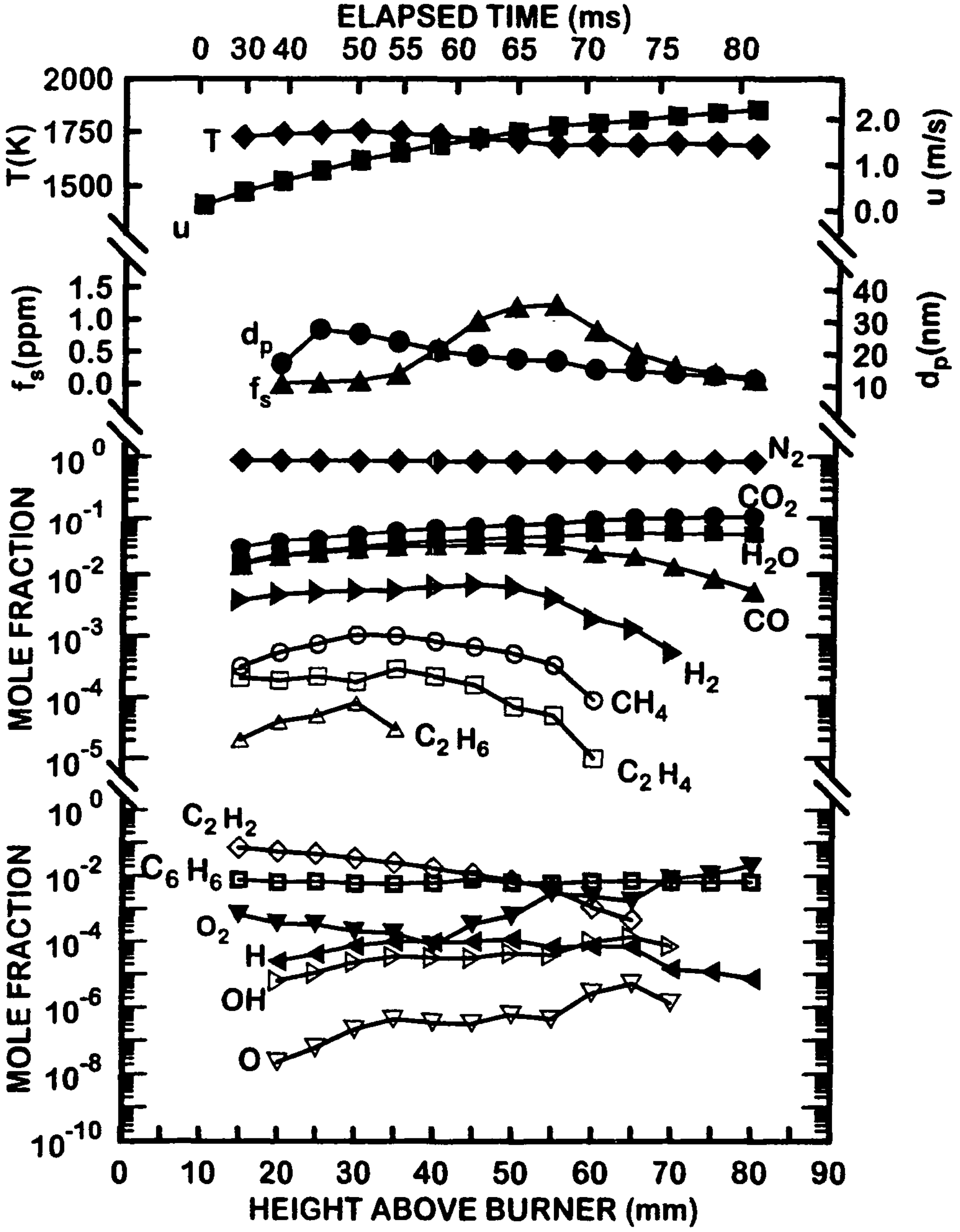
ELAPSED TIME (ms)
0 30 40 50 55 60 65 70 75 80
T(K)
2000
1750
1500
T
u
u (m/s)
2.0
1.0
0.0
f_s(ppm)
1.5
1.0
0.5
0.0
d_p
f_s
d_p(nm)
40
30
20
10
MOLE FRACTION
10^0
10^{-1}
10^{-2}
10^{-3}
10^{-4}
10^{-5}
N_2
CO_2
H_2O
CO
H_2
CH_4
C_2H_6
C_2H_4
MOLE FRACTION
10^0
10^{-2}
10^{-4}
10^{-6}
10^{-8}
10^{-10}
C_2H_2
C_6H_6
O_2
H
OH
O
0 10 20 30 40 50 60 70 80 90
HEIGHT ABOVE BURNER (mm)

7

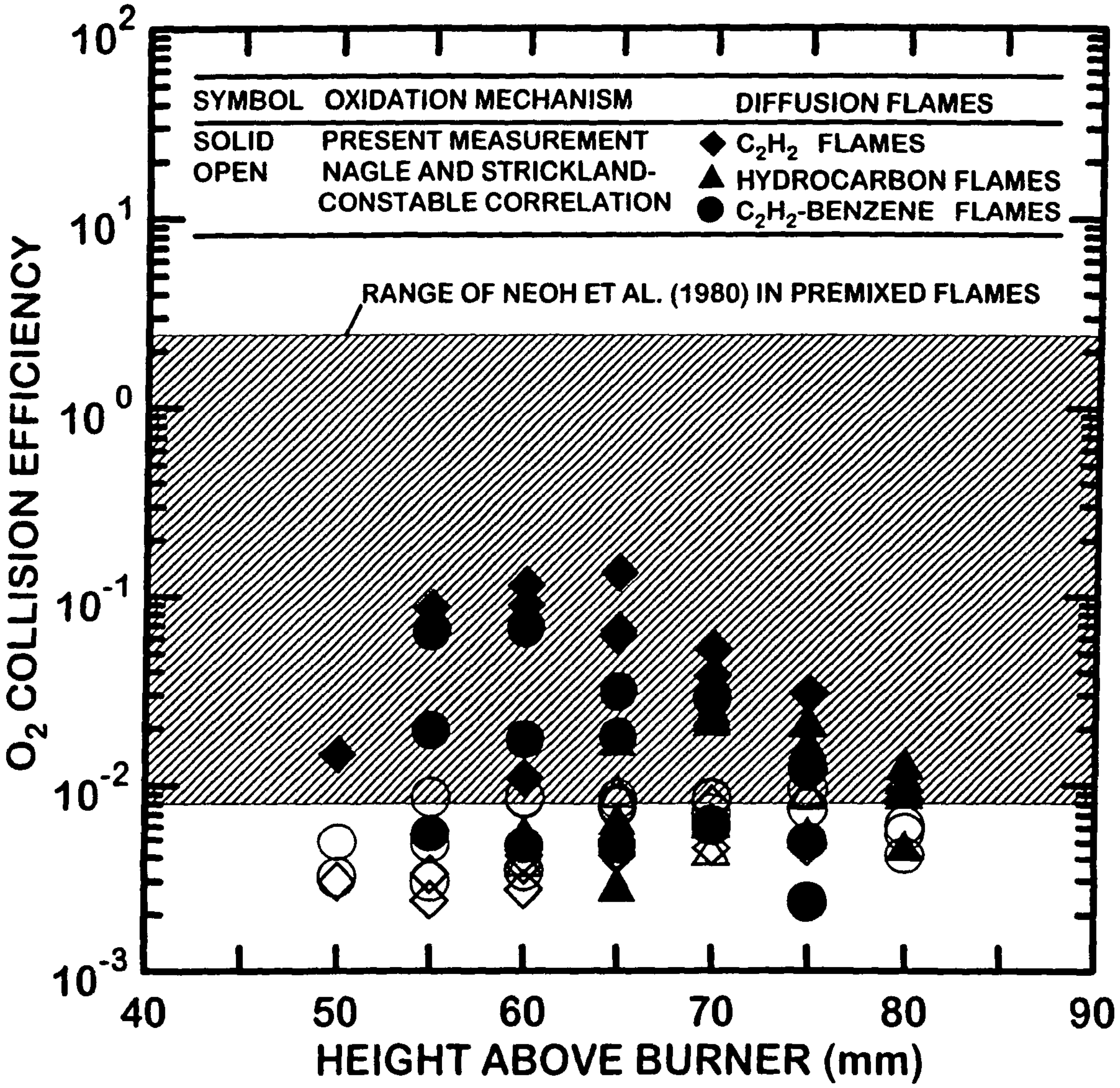
SYMBOL
OXIDATION MECHANISM
DIFFUSION FLAMES
SOLID
OPEN
PRESENT MEASUREMENT
NAGLE AND STRICKLAND-CONSTABLE CORRELATION
◆ C_2H_2 FLAMES
▲ HYDROCARBON FLAMES
● C_2H_2-BENZENE FLAMES
RANGE OF NEOH ET AL. (1980) IN PREMIXED FLAMES
O_2 COLLISION EFFICIENCY
10^2
10^1
10^0
10^{-1}
10^{-2}
10^{-3}
40
50
60
70
80
90
HEIGHT ABOVE BURNER (mm)

(8)

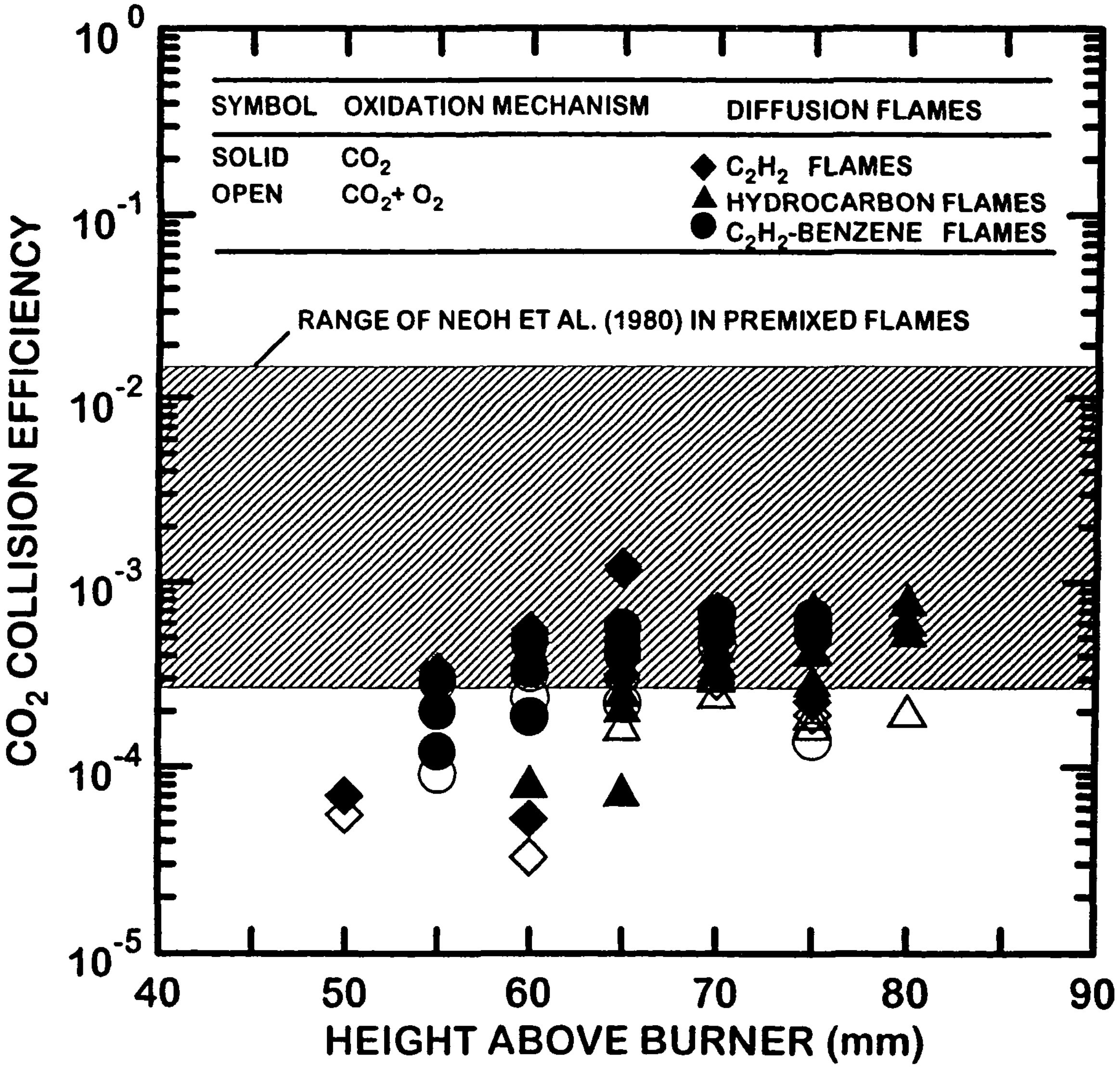
SYMBOL
OXIDATION MECHANISM
DIFFUSION FLAMES
SOLID
CO_2
OPEN
$CO_2 + O_2$
◆ C_2H_2 FLAMES
▲ HYDROCARBON FLAMES
● C_2H_2-BENZENE FLAMES
RANGE OF NEOH ET AL. (1980) IN PREMIXED FLAMES
CO_2 COLLISION EFFICIENCY
10^0
10^{-1}
10^{-2}
10^{-3}
10^{-4}
10^{-5}
40
50
60
70
80
90
HEIGHT ABOVE BURNER (mm)

9

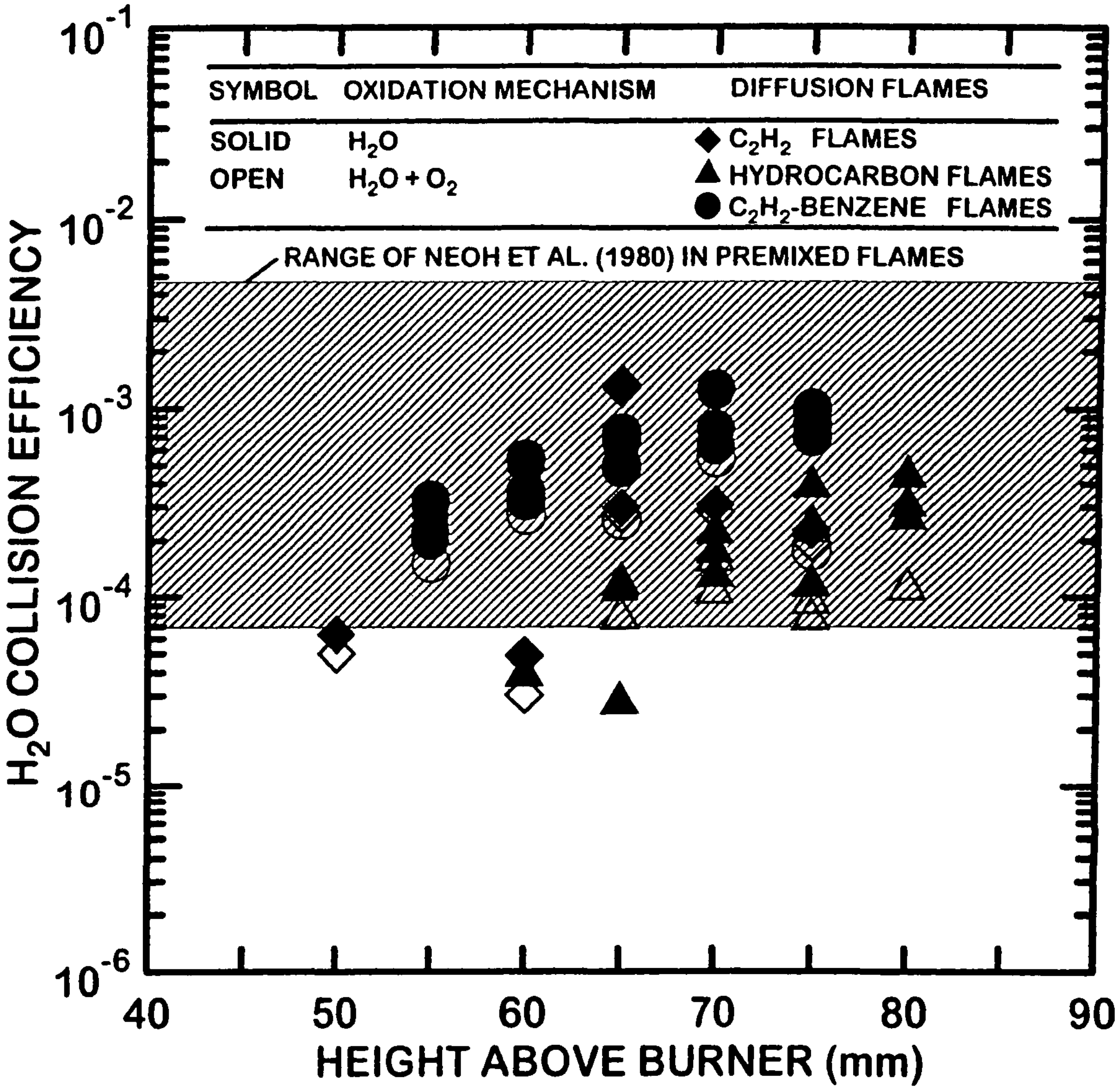
SYMBOL OXIDATION MECHANISM DIFFUSION FLAMES
SOLID H_2O
OPEN $H_2O + O_2$
◆ C_2H_2 FLAMES
▲ HYDROCARBON FLAMES
● C_2H_2-BENZENE FLAMES
RANGE OF NEOH ET AL. (1980) IN PREMIXED FLAMES
10^{-1}
10^{-2}
10^{-3}
10^{-4}
10^{-5}
10^{-6}
H_2O COLLISION EFFICIENCY
40
50
60
70
80
90
HEIGHT ABOVE BURNER (mm)

(10)

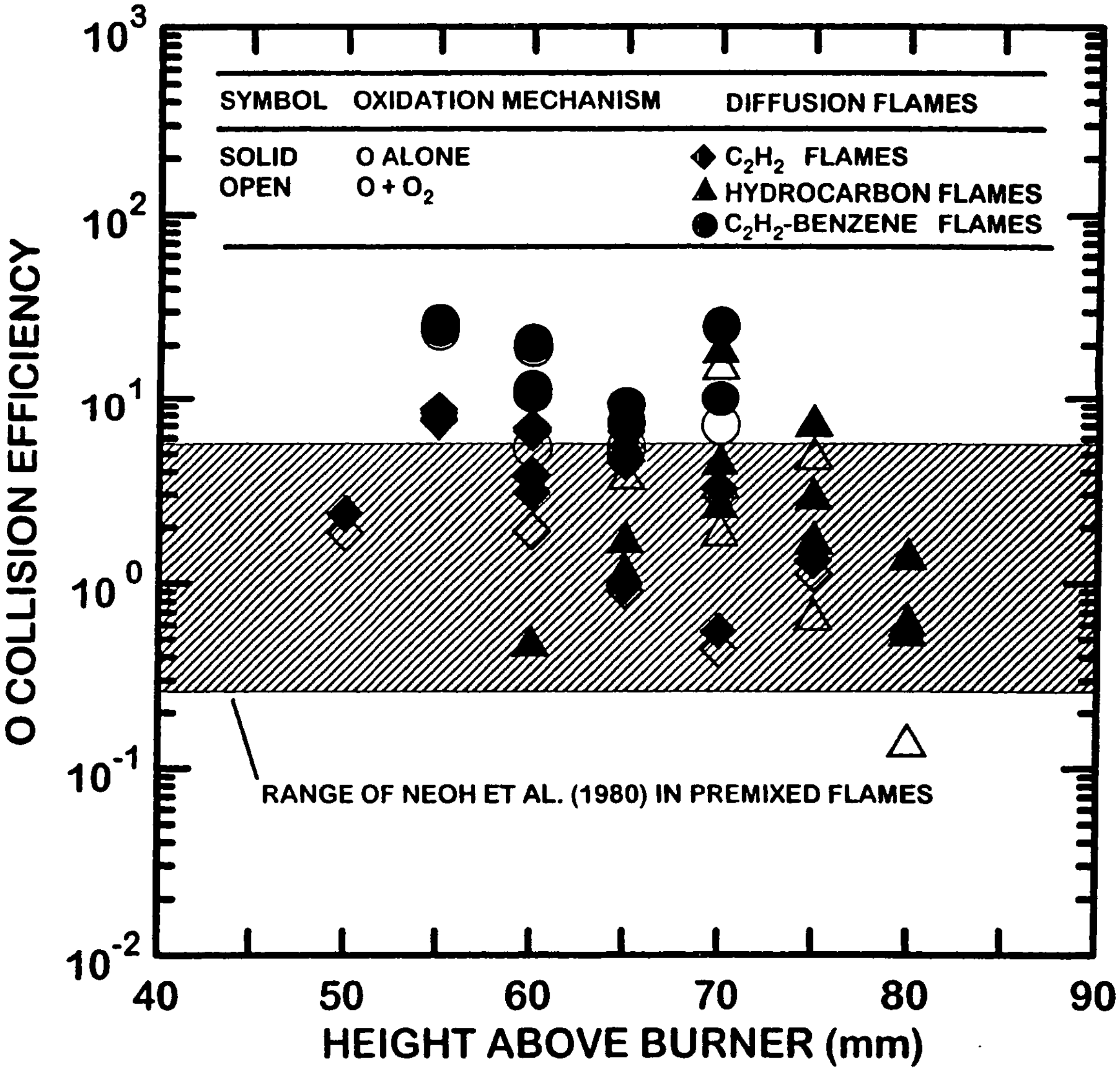

SYMBOL
OXIDATION MECHANISM
DIFFUSION FLAMES
SOLID
O ALONE
OPEN
O + O$_2$
◆ C$_2$H$_2$ FLAMES
▲ HYDROCARBON FLAMES
● C$_2$H$_2$-BENZENE FLAMES
RANGE OF NEOH ET AL. (1980) IN PREMIXED FLAMES
O COLLISION EFFICIENCY
10^{3}
10^{2}
10^{1}
10^{0}
10^{-1}
10^{-2}
40
50
60
70
80
90
HEIGHT ABOVE BURNER (mm)

⑪

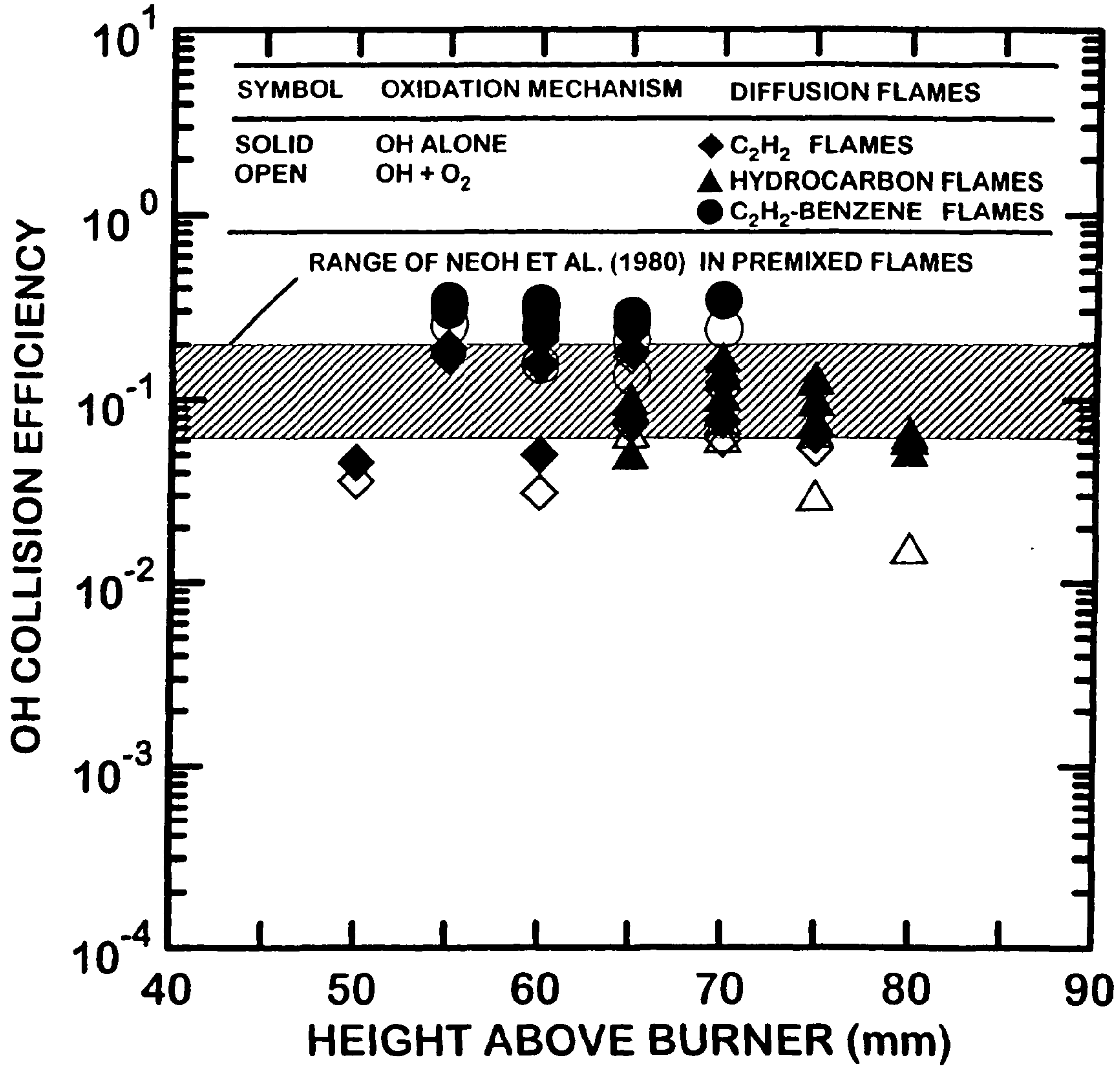
SYMBOL
OXIDATION MECHANISM
DIFFUSION FLAMES
SOLID
OH ALONE
OPEN
OH + O_2
◆ C_2H_2 FLAMES
▲ HYDROCARBON FLAMES
● C_2H_2-BENZENE FLAMES
RANGE OF NEOH ET AL. (1980) IN PREMIXED FLAMES
10^1
10^0
10^{-1}
10^{-2}
10^{-3}
10^{-4}
OH COLLISION EFFICIENCY
40
50
60
70
80
90
HEIGHT ABOVE BURNER (mm)

⑫